Intelligent Maximization of Eco-friendly Output Energy Based on Internal Photovoltaic Structure

Ashraf EL- Bardawil*, Nehad A. Zidan**, Noha H. El-Amary***, W. Abbas***, Mostafa Fedawy****

* Arab Academy for Science, Technology and Maritime Transport, AASTMT, Cairo, Egypt.

** Faculty of Engineering-Mattaria, Helwan University, Cairo, Egypt.

*** Arab Academy for Science, Technology and Maritime Transport, AASTMT, Cairo, Egypt.

****Electronics and Communications Department, Faculty of Engineering, Arab Academy for Science and Technology and Maritime Transport, Cairo, Egypt.

**** Center of Excellence in nanotechnology, Arab Academy for Science and Technology and Maritime Transport, Egypt.

(Eng__ashraf@aast.edu, Nehad2379@yahoo.com, noha_helamary@aast.edu, Wael_abass@aast.edu, m.fedawy@aast.edu)

‡ Ashraf EL- Bardawil; Cairo, Egypt, Tel: +201062079555, Eng__ashraf@aast.edu.

Received: 29.04.2023 Accepted:25.05.2023

Abstract- This paper studies the effect of photovoltaic internal cell structure on the maximization of the overall panel output power. Photovoltaic (PV) power generation is one of the eco-friendly and sustainable electrical energy sources. On the other hand, due to the climate change harmful phenomena, the use of renewable energy resources is mandatory. Henceforward, the manuscript contribution is studying the influence of absorber layer thickness t_p, buffer layer thickness t_n, absorber layer doping N_A, and buffer layer doping N_D on the PV electrical energy management through examining their effect on cell efficiency and panel output power. The simulation is carried out using the SCAPS program. The maximum efficiency and output power are reached by applying three strategies of cell parameters variation (t_p, t_n, N_A and N_D). The simulation results are compared to a market-existing module. A Convolutional Neural Network (CNN) is used to model the PV behavior utilizing the SCAPS results. The obtained results indicate that the module area can be reduced by 22.39 % while maintaining the same power, thereby reducing the overall cost of energy production by the proportion of the land capital cost and maintenance. It indicates satisfying results.

Keywords Convolutional Neural Network (CNN) – Maximum output power (P_{max}) – Open circuit voltage (V_{OC}) –Renewable energy– short circuit current (I_{SC})– solar cell efficiency (η).

1. Introduction

Every day, more solar energy hits the globe than the world's current population can use in a year. Solar energy has multiple advantages; for example, that fact that it is environmentally friendly, as it has no greenhouse emissions. Thus, it is considered a pollution-free energy source. [1].

They are eager to apply the knowledge gained into their everyday lives. An application of that can be seen through the decrease in appeal to non-renewable energy sources due to their various disadvantageous effects on health [1]. Other benefits are economical as using solar energy does not require external energy sources; therefore, it decreases the dependence on foreign sources. Furthermore, it is cost-effective because it requires low maintenance, as solar panels can last for 30 years [2]. In addition, it requires a lot of space to produce the same amount of energy produced by a smaller quantity of fossil fuels.

Gaining expertise in semiconductor physics is essential for improving solar cell efficiency. While altering the electrical and physical properties of the semiconducting silicon material, simulation helps to understand the solar cell device performance [3]. Certain parameters, such as t_p, t_n, N_A and N_D, can be changed using simulation software, which depends on mathematical formulas to estimate the solar cell device performance [4-6]. The thickness of the constituent material is one of the factors that influence the current density voltage properties of solar cells [7-8]. A simulation is used to find the numerical solution of the two-dimensional semiconductor equation, which represents the distribution of electron charge carriers and holes in the simulated solar cell device. It starts with finding the optimal thickness for each layer's performance. Each thickness variation is compared to the other for optimal performance [9].

In order to expand the share of PV electricity in the energy mix in the next years, continuous cost reduction and efficiency improvements of silicon solar cells are critical. While silicon solar cells are becoming more common, efficiency restrictions and improved margins are still present and will be in the future [10]. The characteristics of the a-Si solar cell are determined using a solar cell simulator [11]. The parameters affect a cell's I–V characteristics at any given light intensity and unspecified cell temperature. As a result, they determine the value of performance metrics; such as the short circuit current (I_{SC}), open-circuit voltage (V_{OC}), and the cell's efficiency (η) [12-15].

Energy management describes the approach of regulating and optimizing energy-using systems and producers, to decrease energy consumption per unit of output while still lowering or maintaining the overall system costs [16-20]. Convolutional Neural Network leads to good achievements in some applications. It has evolved into one of the most prominent neural networks in deep learning [21-23]. A CNN is a type of neural network that consists of one or more convolutional layers, often with a subsampling layer, followed by one or more fully connected layers [24-26].

This manuscript illustrates the effect of the structure of Si-based PV technology on the improvement of electrical power generation through the relation between the variation of the PV cell internal parameters and the maximum output power of the module. This study presents a novel contribution in this field, as most of the previous research has studied the effect of ambient temperature and irradiance on photovoltaic performance [10-15] or the sizing and allocation of PV modules on the power system [16-20]. However, in micro-scale studies, most of the research investigates the effect of PV cell internal parameters on PV cell efficiency. CNN is trained to estimate efficiency and maximum output power. Based on these studies, this paper contributes to the state-of-the-art by two main ideas. The first one is the integration between the solar cell internal parameters and the module power. The second one is the involvement of CNN that provides accurate modelling results for a variety of applications. It is used to model the nonlinear behavior of PV internal parameters. The two ideas are not applied in the previous studies that have been illustrated [10-15], and [16-20].

The present paper is organized as follows: Section 1 includes the Introduction, section 2 presents the mathematical model and device structure, section 3 discusses the Simulation study, and section 4illustrates the intelligent CNN model. Finally, section 5 concludes the paper.

2. Mathematical Model

The Solar cell CAPacitance Simulator SCAPS-1D (V.3.3.07) is used to execute the simulation, which has been developed by Pr. Marc Burgelman.et al. [27]. The technique is primarily based on three fundamental equations, including the Poisson equation, the Hole-Continuity equation, and the Electron-Continuity equation [28-30]. The silicon solar cell parameters are shown in Table 1. Conventional Solar cells consist of three layers the absorber layer, the emitter, and the anti-reflecting coating layer, as shown in Fig. 1. The absorber layer is made from P-type silicon. In the p-type absorber layer, the minority and the majority carriers are electrons and holes, respectively. The purpose of this absorber layer is to absorb light. Consequently, minority and majority charge carriers are formed. The emitter layer is essential for charge carrier separation and collection. The emitter layer is made from n-type silicon. The emitter and the absorber layers are linked to form a p-n junction. By diffusion, Electrons flow to the absorber layers, holes move to the emitter layer and a built-in electric field is formed in the junction region. This field causes negatively charged particles to travel one way and positively charged particles to move the other. Thus, one can say that the emitter layer functions as a selective membrane that allows minority charge carriers to move through. The membrane resists the movement of the majority carriers. Without the emitter layer, generated charge carriers would simply roll around in the absorber layer until they recombine. An anti-reflection coating is placed at the front of the cell to reduce the front surface reflection and maximize the transmission probability into the cell. Finally, metallic contacts, or electrodes, are needed at both sides of the solar cell to collect these carriers and send them to an external circuit. Up to 500µm is the maximum size of an ideal silicon solar cell with excellent light trapping (base) and up to 1.5 µm for n-layer. Up to 500µm is the maximum size of an ideal silicon solar cell with excellent light trapping (base), and up to 1.5 µm for n-layer. The main parameters that are used to characterize the performance of solar cells are the open circuit voltage V_{OC} , the short-circuit current density J_{SC} and power conversion Efficiency.

$$J_{SC} = -J_{ph} + J_d \tag{1}$$

Where (J_{ph}) is the photocurrent density; and (J_d) is the diode current density.

$$J_d = J_0\left[e^{\frac{qV}{nkT}} - 1\right] \tag{2}$$

$$J_{SC} = J_0\left[e^{\frac{qV}{nkT}} - 1\right] - J_{ph} \tag{3}$$

$$V_{OC} = \frac{nkT}{q}\,\mathrm{LN}\left[\frac{I_L}{I_0} + 1\right] \tag{4}$$

Where I_L is the light generated current, the open-circuit voltage corresponds to the amount of forward bias on the solar cell due to the bias of the solar cell junction with the light generated current. Selecting a material with a higher band gap (E_g) the reverse saturation current can be reduced.

$$\eta = \frac{V_{oc}\ \ I_{sc}\,FF}{P_{in}} \tag{5}$$

Where FF is the fill factor and P_{in} is the input power, the solar cell is designed at Standard Test Condition (STC) where the irradiance (P_{in}) is 1000W/m², cell temperature is 25°C, and Air Mass (AM1.5).

$$V_{module} = v_{cell} * N_{cell} \tag{6}$$

$$P_{module} = V_{module} * I_{module} \tag{7}$$

$$\text{Increase of power }(\%) = \left(\frac{P_{max} - P_{tallmax}}{P_{tallmax}}\right) * 100 \tag{8}$$

Where V_{module} is the module voltage, N_{cell} is the number of series cells, I_{module} is the module current, P_{module} is the module power, $P_{tallmax}$ is the power of existing module; and P_{max} is the maximum power for each strategy.

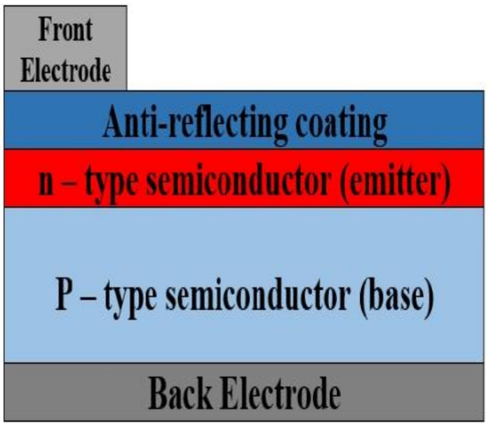

Fig. 1. Basic structure of the solar cell.

Table 1. Parameters of SI solar cell

Description	Value
Bandgap (eV)	1.13
Electron affinity (eV)	4.5
Dielectric permittivity	11.9
Conduction band (CB) (cm^{-3})	2.890E+19
Valence band (VB) (cm^{-3})	3.140E+19
Electron velocity (cm/s)	2.030E+7
Hole velocity (cm/s)	1.670E+7
Electron mobility (cm²/Vs)	1.410E+3
Hole mobility (cm²/Vs)	4.770E+2

3. Simulation Study

The aim of this paper is to study the factors that limit the performance of Si-based solar cells. The influence of the (t_p, N_A, t_n and N_D) are examined. The results are compared with a market-existing module (TALLMAX), in which the parameters of the practical module are shown in Table 2.

Table 2. Parameters of the particle module

Description	Value
Cell orientation	72 cells
Solar cell (mm)	156.75 × 156.75
Module Dimensions (mm)	1956 × 992 × 40
Open Circuit Voltage-V_{OC} (V)	46.3
Short Circuit Current I_{SC} (A)	9.39
Maximum Power Voltage V_{mPP} (V)	37.6
Maximum Power Current I_{mPP}(A)	8.91
Maximum Power P_{max}(W)	335
Module Efficiency η (%)	17.3

The work is progressed through three strategies as shown in Fig.2.

1. The first strategy: in which the impact of the solar cell parameters' variation on the module maximum Power (P_{max}) and module efficiency (η) is tested starting from t_n, t_p, N_A to N_d.
2. The second strategy: in which the impact of the solar cell parameters' variation is tested starting from N_d, N_A , t_p to t_n (versa vice the first strategy sequence).
3. The third strategy: in which the parameters are varied to find the optimum arrangement that gives P_{max}.

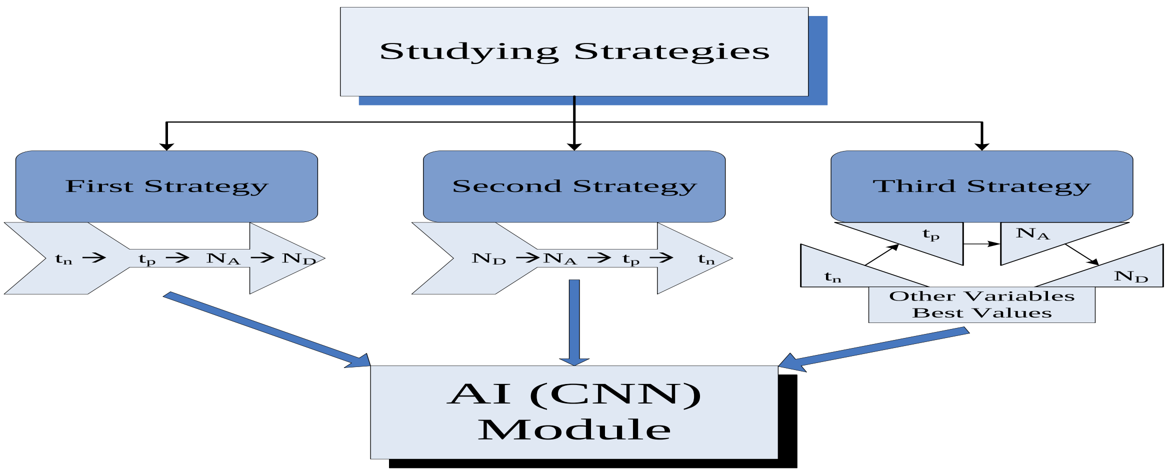

Fig. 2. Three strategies of cell parameters variation.

A. The First strategy:

I. Buffer layer thickness ($\boldsymbol{t_n}$)

The thickness of buffer layer is varied from 0.1 μm up to 2 μm with constant $t_p = 200$ μm , $N_A = 10^{16}\ cm^{-3}$ and $N_D = 10^{16}\ cm^{-3}$. Fig. 3 shows the relation between the buffer layer thickness (in μm) and Efficiency ɳ (%) and maximum power (P_{max} in W). It is obvious from Fig.3 that the efficiency decreases linearly as the buffer layer thickness increases. P_{max} decreases linearly with $\mathrm{t_n}$ until $\mathrm{t_n} = 1.5$μm. It is cleared that the maximum efficiency and maximum power are reached at $\mathrm{t_n} = 0.1$ μm, which are fixed in the other parameters test.

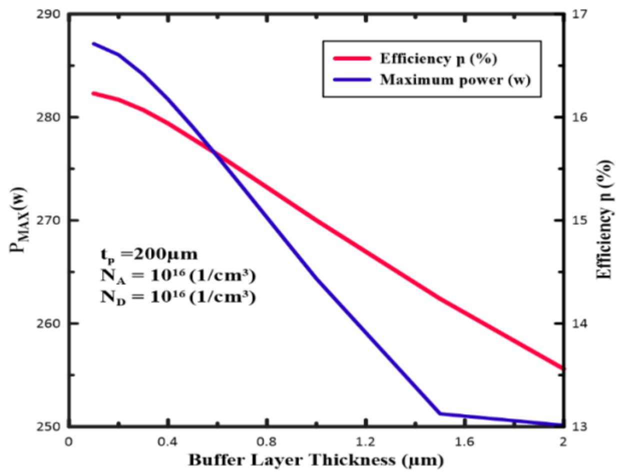

Fig. 3. Buffer layer thickness vs Efficiency and maximum power.

II. Absorber layer thickness ($\boldsymbol{t_p}$)

The thickness of the absorber layer ranges from 50 μm to 1000 μm with constant $t_n = 0.1$ μm , $N_A = 10^{16}\ cm^{-3}$, and $N_D = 10^{16}\ cm^{-3}$. The relation between the absorber layer thickness (in μm) P_{max} and efficiency ɳ is presented in Fig.4. It is perspicuous that P_{max} and ɳ increase almost exponentially with t_p. The range of 250-350 μm is the preferred and the optimal t_p.

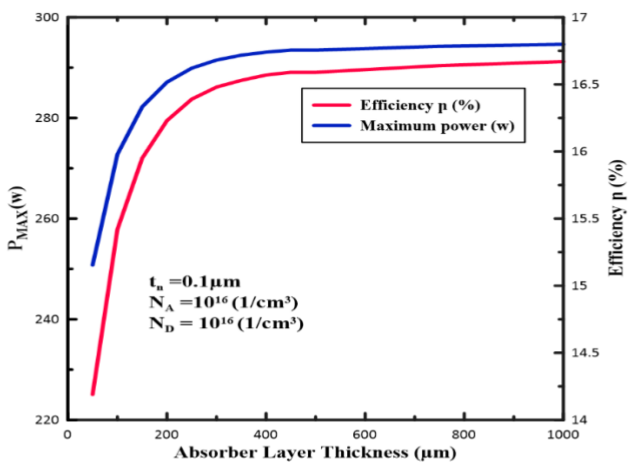

Fig. 4. Absorber layer thickness vs maximum power and efficiency.

III. Absorber layer doping ($\boldsymbol{N_A}$)

The absorber layer doping ranges from $10^{14}\ cm^{-3}$ to $10^{20}\ cm^{-3}$ with constant $t_n = 0.1$ μm , $t_p = 300$ μm and $N_D = 10^{16}\ cm^{-3}$. Fig. 5 represents the absorber layer doping (in cm^{-3}) vs ɳ and P_{max}. P_{max} and ɳ increase linearly with N_A till 10^{15} . As N_A is greater than $10^{16}\ cm^{-3}$, ɳ and P_{max} become saturated. It is cleared that $N_A = 10^{18}\ cm^{-3}$ gives the maximum values of ɳ and P_{max}.

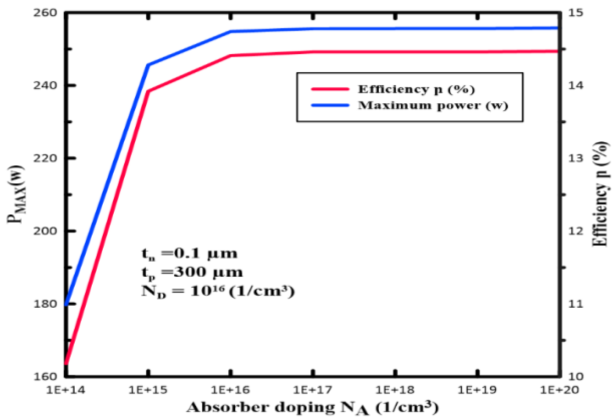

Fig. 5. Absorber layer doping vs efficiency ɳ and maximum power.

IV. Buffer layer doping ($\boldsymbol{N_D}$)

The buffer layer doping is varied from $10^{14}\ cm^{-3}$ up to $10^{20}\ cm^{-3}$ with constant $t_n = 0.1$ μm , $t_p = 300$ μm and $N_A = 10^{18}\ cm^{-3}$. Fig. 6 shows the buffer layer doping (in cm^{-3}) vs ɳ and P_{max}. P_{max} and ɳ increase linearly with N_D untill 10^{19}; afterward, they become nearly saturated. The maximum value of P_{max} and ɳ are reached as $N_D = 10^{20}\ cm^{-3}$. It is noticed that there is a similarity in the variation behavior of the four parameters (t_n,t_p,N_A, and N_D) with both P_{max} and ɳ.

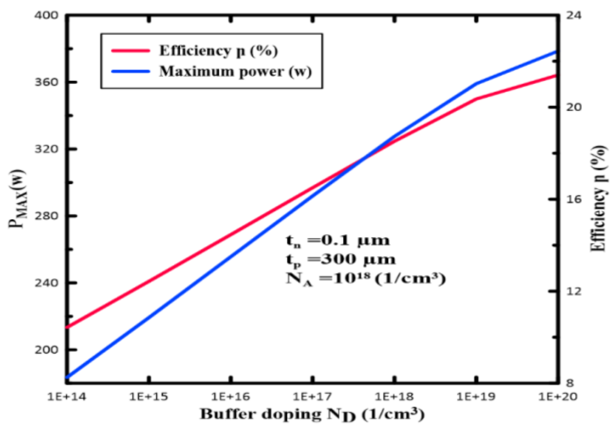

Fig. 6. Buffer layer doping vs efficiency ɳ and maximum power.

The P-V and I-V curves for this case are shown in Fig.7 (a & b) compared to those of the market module. The maximum power P_{max} increases to 380 W. Table 3 clarifies the parameters of the studied module.

Table 3. Parameters of the first strategy module

Open Circuit Voltage-V_{OC} (V)	50.9
Short Circuit Current I_{SC} (A)	8.85
Maximum Power Voltage V_{mPP} (V)	44.65
Maximum Power Current I_{mPP}(A)	8.476
Peak Power P_{max}(W)	380
Module Efficiency ɳ (%)	21.5

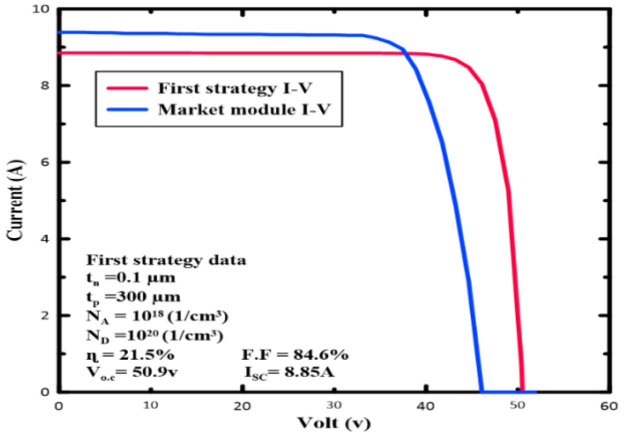

(a)

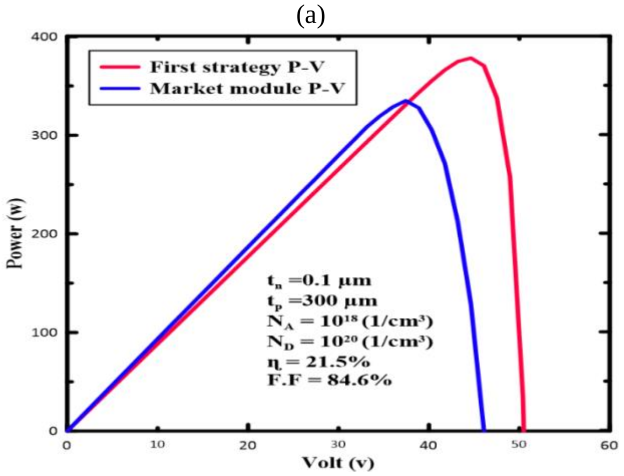

(b)

Fig. 7. (a) Module current vs voltage, (b) Module power vs voltage.

B. Second strategy:

Using the same behavior as the first strategy, but in reverse sequence, the results of the second strategy are determined.

I. Buffer layer doping ($\boldsymbol{N_D}$)

The buffer layer doping is changed with constant $t_n = 0.3$ µm , $t_p = 150$ µm and $N_A = 10^{16}\ cm^{-3}$. Fig. 8 exhibits $N_D$vs P_{max}. P_{max} increases linearly with N_D untill 10^{17} then it becomes nearly saturated. The maximum value of P_{max} is reached at $N_D = 10^{18}\ cm^{-3}$, which is considered in the rest of the strategy steps.

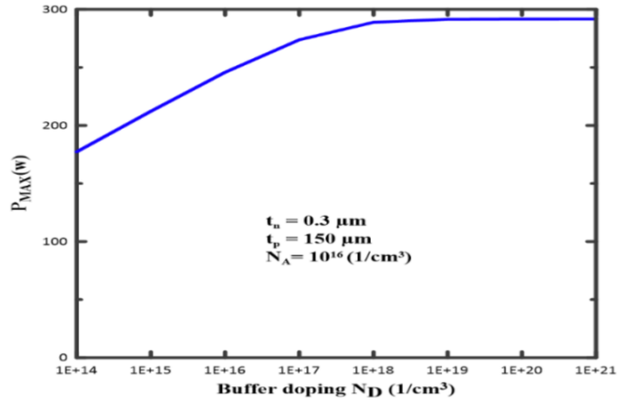

Fig. 8. Buffer layer doping vs maximum power.

II. Absorber layer doping ($\boldsymbol{N_A}$)

The absorber layer doping is varied with constant $t_n = 0.3$ µm , $t_p = 150$ µm and $N_D = 10^{18}\ cm^{-3}$. Fig. 9 shows N_A vs P_{max}. P_{max} increases linearly with N_A till it reaches its maximum value at $N_A = 10^{18}\ cm^{-3}$.

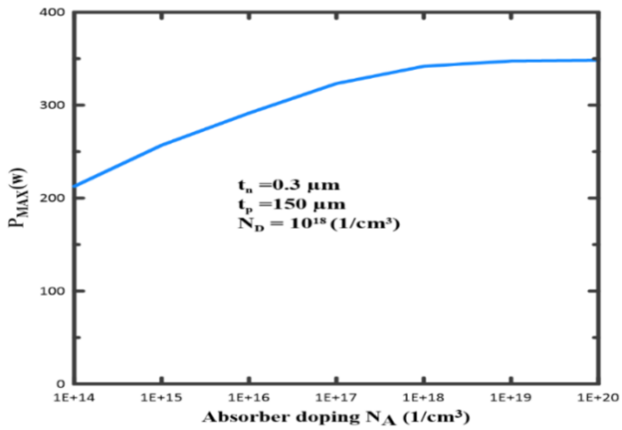

Fig. 9. Absorber layer doping vs maximum power.

III. Absorber layer thickness ($\boldsymbol{t_p}$)

The thickness of the absorber layer ranges from 50 µm to 500 µm with constant $t_n = 0.3$ µm , $N_A = 10^{18}\ cm^{-3}$ and $N_D = 10^{18}\ cm^{-3}$. Fig. 10 illustrates the relation between t_p and P_{max}. The range of $t_p = 200 - 300$µm is the preferred absorber layer thickness. P_{max} becomes saturated after $t_p = 300$ µm.

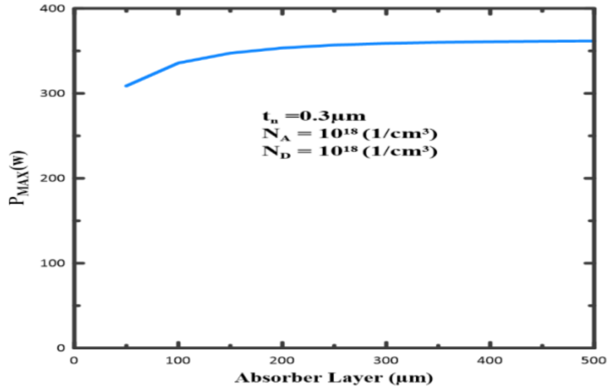

Fig. 10. Absorber layer thickness vs maximum power.

IV. Buffer layer thickness (t_n)

The thickness of buffer layer is varied with constant $t_p = 300$ µm , $N_A = 10^{18}\ cm^{-3}$ and $N_D = 10^{18}\ cm^{-3}$. Fig. 11 represents the relation between t_n and P_{max}. It is obvious that P_{max} decreases linearly with t_n. It is clearly that P_{max} reaches its maximum value at $t_n = 0.1$ µm.

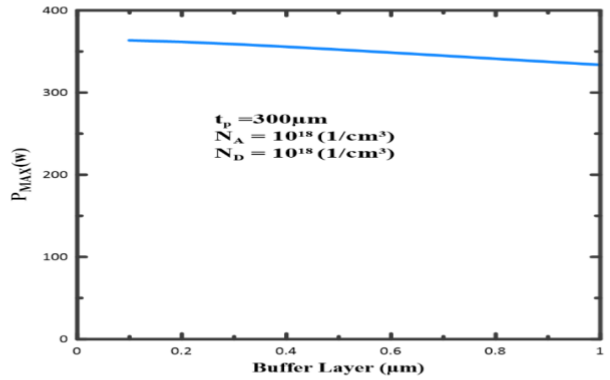

Fig. 11. Buffer layer thickness vs maximum power.

Fig. 12 (a & b) clarifies the P-V curve and I-V curve for the second strategy compared to the market module. The maximum P_{max} equals 363 W. It decreases compared to the first strategy, while both are greater than the original panel value. Table 4 indicates the parameters of the studied module.

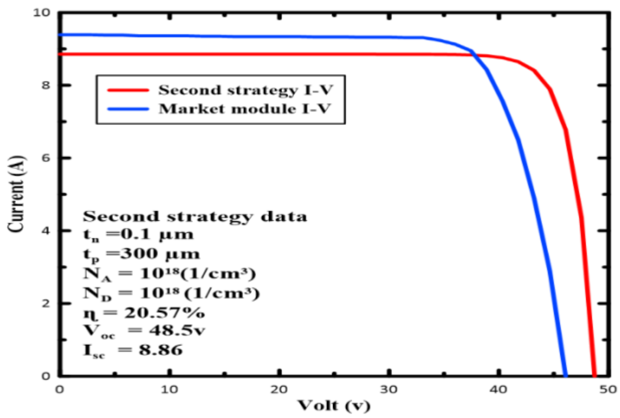

(a)

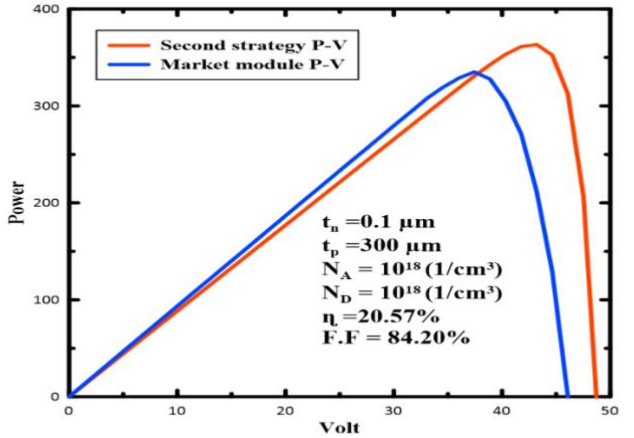

(b)

Fig. 12. (a) Module current vs voltage, (b) Module power vs voltage.

Table 4. Parameters of the second strategy module

Open Circuit Voltage-V_{OC} (V)	49
Short Circuit Current I_{SC} (A)	8.86
Maximum Power Voltage V_{mPP} (V)	43.2
Maximum Power Current I_{mPP}(A)	8.4
Peak Power P_{max}(W)	363
Module Efficiency ŋ (%)	20.57

C. Third strategy:

I. Buffer layer thickness (t_n)

By selecting the best values of $N_A = 10^{19}\ cm^{-3}$ and $N_D = 10^{20}\ cm^{-3}$ from the first strategy and assigning $t_p = 250$ µm, it is found that the maximum P_{max}. is at $t_n = 0.1$ µm.The variation of P_{max} with the buffer layer thickness t_n is shown in Fig.13.

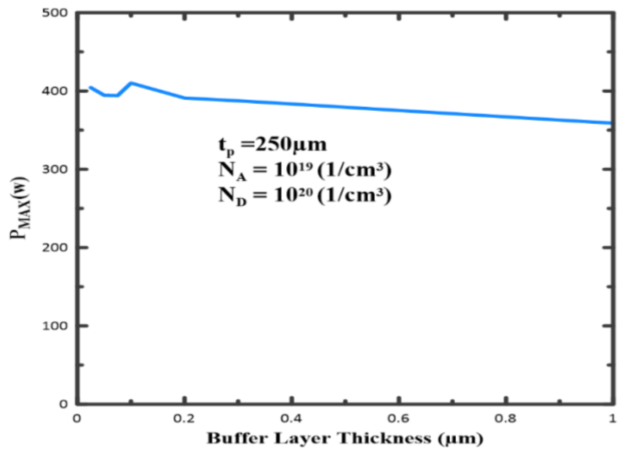

Fig. 13. Buffer layer thickness vs maximum power.

II. Absorber layer thickness (t_p)

The thickness of the Absorber layer (t_p) is varied with constant $t_n = 0.1$ µm , $N_A = 10^{19}\ cm^{-3}$ and $N_D = 10^{20}\ cm^{-3}$. Fig. 14 illustrates that 250µm is the optimized t_p. The variation after this value of t_p causes unconsidered increase in P_{max}.

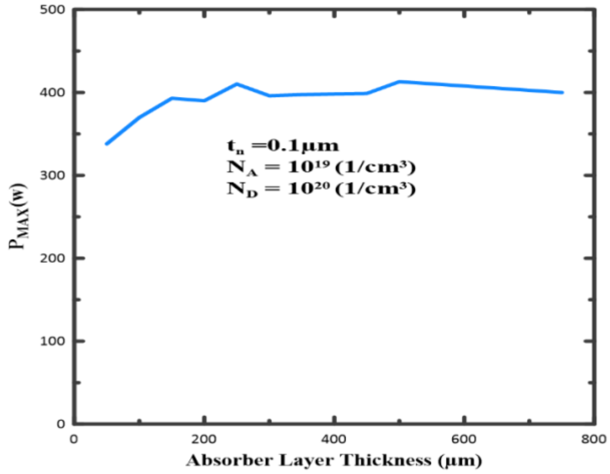

Fig. 14. Absorber layer thickness vs maximum power.

III. Absorber layer doping (N_A)

As the absorber layer doping (N_A) is changed with constant $t_n = 0.1$ µm , $t_p = 250$ µm and $N_D = 10^{20}\ cm^{-3}$, the maximum P_{max} is observed at $N_A = 10^{19}\ cm^{-3}$ as presented in Fig.15.

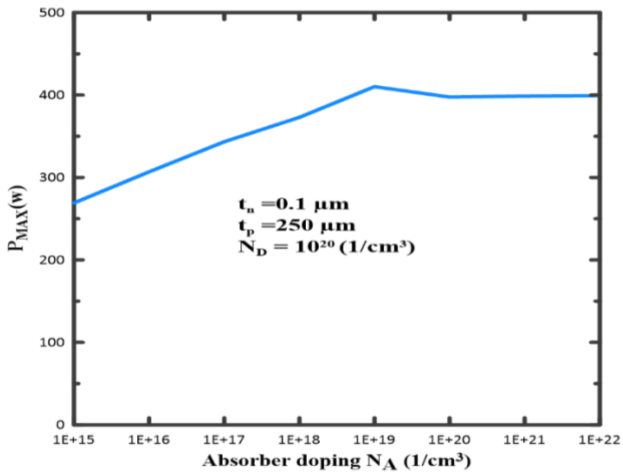

Fig. 15. Absorber layer doping vs maximum power.

IV. Buffer layer doping (N_D)

As the buffer layer doping (N_D) is varied with constant $t_n = 0.1$ µm , $t_p = 250$ µm and $N_A = 10^{19}\ cm^{-3}$, the highest P_{max} is observed at $N_D = 10^{20}\ cm^{-3}$ as clarified in Fig.16 . The P-V and I-V curves for the third strategy relative to the market module are shown in Fig.17 (a & b). The maximum P_{max} increases to 410 W. Table 5 shows the value of the studied module.

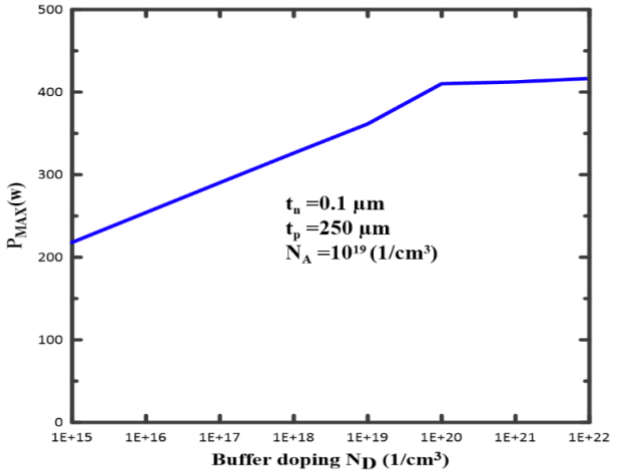

Fig. 16. Buffer layer doping vs maximum power.

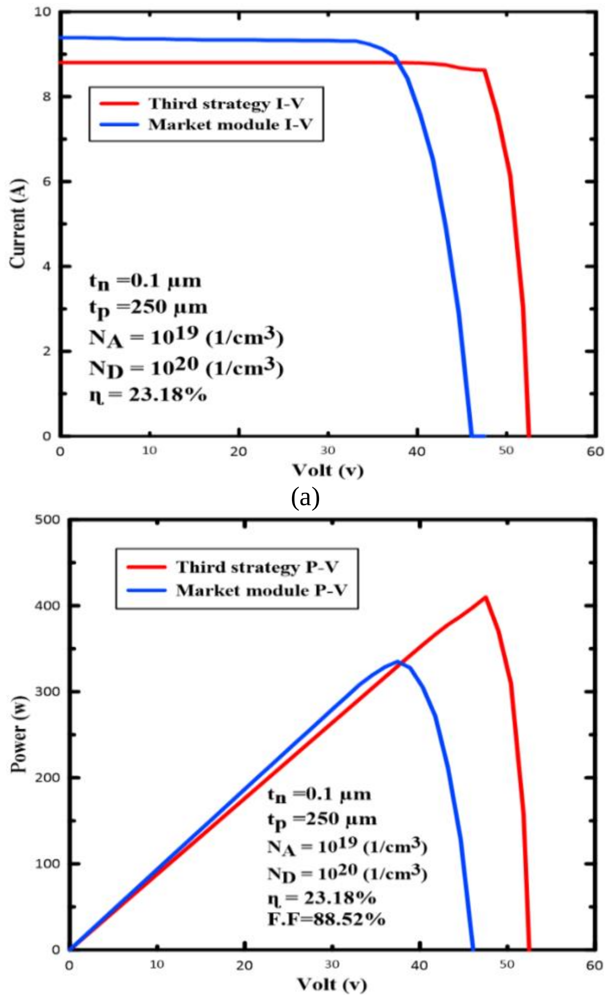

Fig. 17. (a) Module current vs voltage, (b) Module power vs voltage.

Table 5. Parameters of the third strategy module

Open Circuit Voltage-V_{OC} (V)	53.28
Short Circuit Current I_{SC} (A)	8.8
Maximum Power Voltage V_{mPP} (V)	47.52
Maximum Power Current I_{mPP}(A)	8.63
Peak Power P_{max}(W)	410
Module Efficiency ɳ (%)	23.18

Table 6 and Fig.18 illustrate a comparison between the parameters of the existing module and the output performance of the three strategies. For the same module area, the best cell efficiency (ɳ) is obtained from the third strategy to be 23.18% instead of 17.3% of the existing market module. Furthermore, P_{max} is improved from 335 W to 410 W with an increased power percentage equal to 22.39%. It means that for the same power, the module area can be reduced by 22.39% to reduce the overall cost of electricity generation by the share of land capital cost and the maintenance of the reduced area.

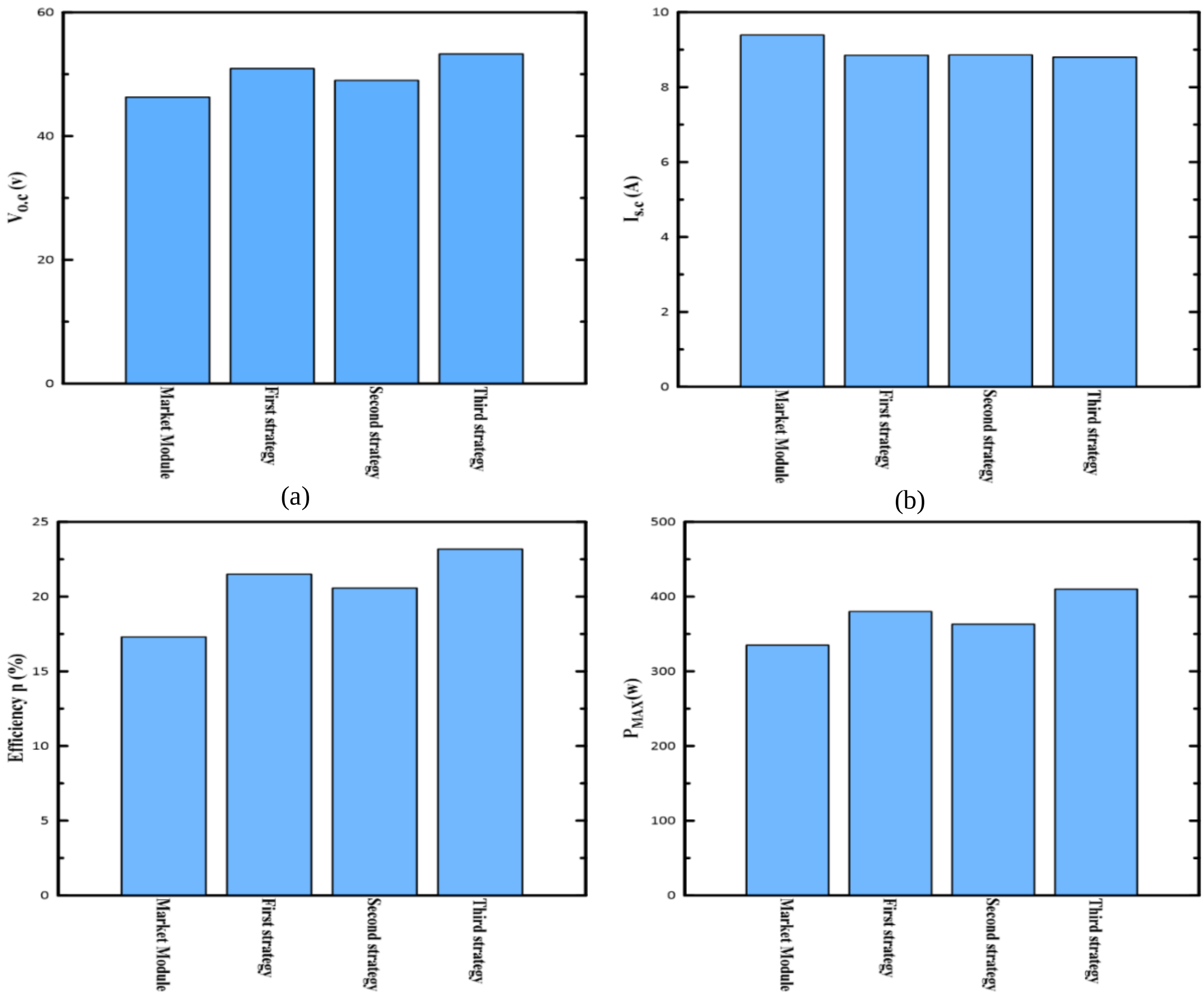

(c) (d)

Fig. 18. (a) Solar panel open circuit voltage for different strategies, (b) Solar panel short circuit current for different strategies, (c) Solar panel efficiency for different strategies and (d) Solar panel maximum power for different strategies

Table 6. Different modules parameters comparative table

	Market module	First strategy	Second strategy	Third strategy
V_{OC} (V)	46.3	50.9	49	53.28
I_{SC} (A)	9.39	8.85	8.86	8.8
V_{mPP} (V)	37.6	44.65	43.2	47.52
I_{mPP}(A)	8.91	8.476	8.4	8.63
Area (mm^2)	1956 × 992	1956 × 992	1956 × 992	1956 × 992
Efficiency ɳ (%)	17.3	21.5	20.57	23.18
P_{max}(W)	335	380	363	410
Increase of power (%)	-	13.43	8.36	22.39

4. Intelligent CNN Model

CNN fulfills good modelling results for different applications, it is used to model the non-linear PV internal parameters behavior. The system is built with four input data features (t_n, t_p, N_A and N_d) and two output variable layers (P_{max},η). The dataset used to train and test the proposed system is created using SCAPS. The system is trained and tested using 350 and 50 samples respectively.

The developed CNN consists of 11 layers which are the image input layer, the convolution 2-d layer, fully connected one, and the output layer as illustrated obviously in Fig.19. The convolution layer is the fundamental component of a CNN. It bears the bulk of the network's computational strain. This layer performs a dot product between two matrices, one of which represents the set of learnable parameters. The Swish layers illustrate the relevance of activation functions. The fully connected layer facilitates the mapping between the input and output representations. Fig. 20 (a, b) shows the values of predicted and original efficiency and power respectively. The Root Mean Square Error (RMSE) for efficiency is 0.08 and RMSE for maximum power is 0.95. Referring to the fact that CNNs typically perform well with grid-like datasets or structured data formats, it is the main initiative behind utilizing it in this study. CNNs can also take advantage of local connectivity and shared weights in the input, by using convolution layers that apply filters to very small local regions of the dataset, which allow them to capture small local regions of the input data that are relevant to the regression analysis.

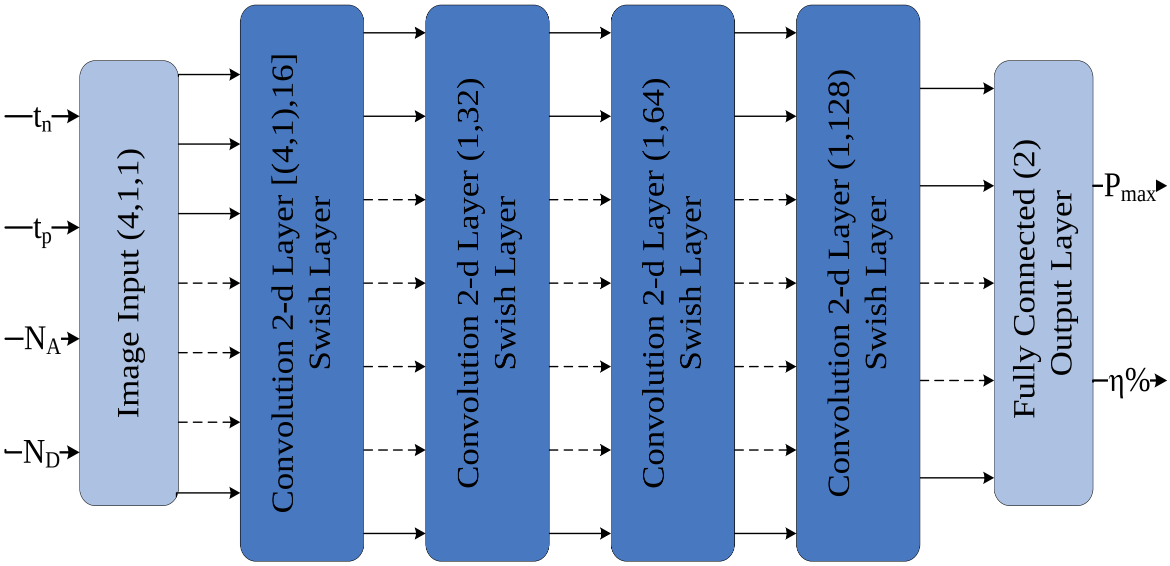

Fig. 19. The convolution neural network architecture.

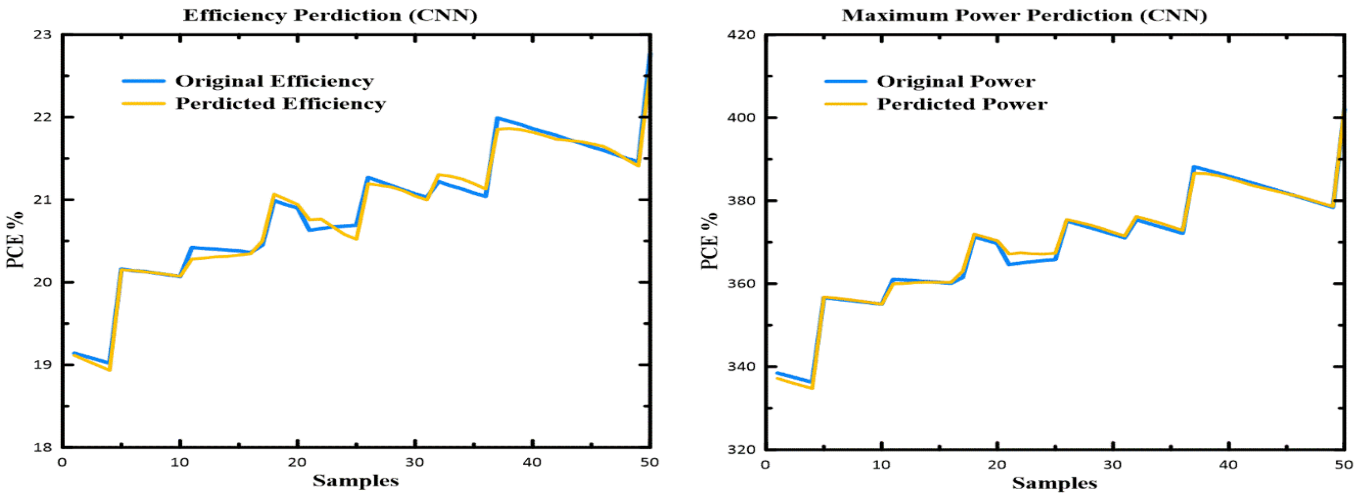

(a) (b)

Fig. 20. (a) The predicted and original efficiency variation with the test samples using CNN, (b) The predicted and original power variation with the test samples using CNN.

5. Conclusion

According to the integration of studies in renewable energy field, this research connects the micro-scale studies of the PV cell parameters with the macro-scale energy management systems. The contribution of this work depends on two main points, which are: 1- studying the impact of the variation of the solar cell internal parameters on the module overall output power, and 2- emulating the system using

CNN. The investigation fact of PV cell internal parameters effect on maximizing the output power and minimizing the unit cost. The simulation is verified within three strategies,

all strategies depend on the variation of (t_n, t_p, N_A and N_d) sequentially using SCAPS program.

i. The first strategy arranges the variation of the parameters as (t_n, t_p, N_A and N_d) to increase P_{max} by 13.43% at $\eta = 21.5\%$.
ii. The second strategy is opposite to the first strategy according to the parameter sequence to boost P_{max} by 8.36% at $\eta = 20.57\%$.
iii. The third strategy involves varying the parameters logically and sequentially to obtain the optimum arrangement to give the highest efficiency and the highest maximum output power, which is P_{max} raised by 22.39% at $\eta = 23.18\%$.

The obtained results show that the module area can be minimized by 22.39% for the same power as described in the third strategy. As a result, lowering the overall cost of energy generation by the proportion of the land capital cost and maintenance. CNN is designed to model the relation between the PV internal parameters (t_n, t_p, N_A and N_d) and the maximum output power and efficiency. Furthermore, the intelligent network error percentage ranges between 0.25% - 0.27%.

Acknowledgements

This work is supported by the Center of Excellence in Nanotechnology, Arab Academy for Science and Technology and Maritime Transport (AASTMT), Cairo, Egypt.

References

[1] D. Muradin, “Advantages and disadvantages of renewable energy sources utilization” IJEEP , DOI: 10.32479/ijeep.11027, Vol. 11, No. 3, pp. 176–183, April 2021.

[2] H. H. Goh, C. Li, D. Zhang, W. Dai, C. S. Lim, T. A. Kumiawan, K. C. Goh, “Application of choosing by advantages to determine the optimal site for solar power plants” Scientific Reports, DOI: 10.1038/s41598-022-08193-1, Vol. 12, pp. 1-16, March 2022.

[3] L. C. Andreani, A. Bozzola, P. Kowalczewski, M. Liscidini, and L. Redorici, “Silicon solar cells: toward the efficiency limits” Advances in Physics: X, DOI: 10.1080/23746149.2018.1548305, Vol. 4, pp. 25-48, January 2019.

[4] A. Fell, J. Schön, M. C. Schubert, and S. W. Glunz, "The concept of skins for silicon solar cell modeling" Solar Energy Materials and Solar Cells, DOI: 10.1016/j.solmat.2017.05.012, vol. 173, pp. 128-133, December 2017.

[5] A. Fell, K. R. McIntosh, P. P. Altermatt, G.J. M. Janssen, R.Stangl, A. Ho-Baillie, J. Greulich, M. Müller, B. Min, K. C. Fong, M. Hermle, I. G. Romijn, M. D. Abbott, “Input Parameters for the Simulation of Silicon Solar Cells in 2014” IEEE J. Photovoltaics, DOI: 10.1109/JPHOTOV.2015.2430016, Vol. 5, pp. 1250–1263, July 2015.

[6] V. Yadav, S. Kashyap, R. Pandey and J. Madan, "Influence of Absorber Thickness on the Performance of Sb2S3 based Solar Cell using Numerical Simulations," 2nd Edition of IEEE Delhi Section Flagship Conference (DELCON), Rajpura, India, pp. 1-5, February 2023.

[7] J. Zhou, Y. Tan, W. Liu, X. Cai, H. Huang, and Y. Cao, “Effect of front surface light trapping structures on the PERC solar cell” SN Appl. Sci., DOI: 10.1007/s42452-020-2608-4, Vol. 2, No. 5, pp. 799, May 2020.

[8] N. A. Mahammedi, H. Gueffaf, B. Lagoun and M. Ferhat “Numerical simulation and optimization of a silicon clathrate-based solar cell n-Si136/p-Si2 using SCAPS-1D program” Optical Materials, DOI: 10.1016/j.optmat.2020.110043, Vol. 107, pp. 1-7, September 2020.

[9] E. Purwandari, S. Mutma’inah, W. Maulina, A. Arkundato, L. Rohman and R. D. Syarifah, “Simulation of Hydrogenated Amorphous Silicon-based Solar Cell: Investigation of J-V Characteristic in Optimum Thickness” Journal of Physics: Conference Series, Vol. 1951, No. 1, pp. 1-7, June 2021.

[10] K. Sopian, S. L. Cheow, and S. H. Zaidi, “An overview of crystalline silicon solar cell technology: Past, present, and future” 4th International Conference on the Advancement of Materials and Nanotechnology, Vol. 1877, pp. 1-11, 2017.

[11] S. Chander, A. Purohit, A. Sharma, Arvind, S. P. Nehra and M. S. Dhaka “A study on photovoltaic parameters of mono-crystalline silicon solar cell with cell temperature” Energy Reports, DOI: 10.1016/j.egyr.2015.03.004, Vol. 1, pp. 104–109, November 2015.

[12] M. Savadogo, B. Soro, R. Konate, I. Sourabié, M. Zoungrana, I. Zerbo, D. J. Bathiebo “Temperature Effect on Light Concentration Silicon Solar Cell’s Operating Point and Conversion Efficiency,” SGRE, DOI: 10.4236/sgre.2020.115005, Vol. 11, No. 05, pp. 61–72, May 2020.

[13] F. Javed, “Impact of Temperature & Illumination for Improvement in Photovoltaic System Efficiency,” INTERNATIONAL JOURNAL of SMART GRID, DOI: 10.20508/ijsmartgrid.v6i1.222.g185, Vol.6, No.1, March 2022.

[14] A. Raturi, P. Mittal and S. Choudhary, "Density functional characterization of electronic and optical properties of strontium titanate under doping and strain for optoelectronic applications," in IEEE Transactions on

Nanotechnology, DOI: 10.1109/TNANO.2023.32800832023.

[15] D. R. Ahmed, I. R. Mohammed, H. M. Abdullah, F. F. Muhammadsharif, K.Sulaiman, M. S. Alsoufi, T. M. Bawazeer, "The Correlation of Device Parameters with Illumination Energy to Explore the Performance of a Monocrystalline Silicon Solar Module" Silicon, DOI: 10.1007/s12633-021-00966-z, Vol. 14, No. 4, pp. 1439–1445, Feberuary 2022.

[16] Y. E. G. Vera, R. Dufo-López, and J. L. Bernal-Agustín, "Energy Management in Microgrids with Renewable Energy Sources: A Literature Review" Applied Sciences, DOI: 10.3390/app9183854, Vol. 9, No. 18 pp. 1-28, September 2019.

[17] H. K. Khalil, S. M. Yousri and N. H. El-Amary, "Smart Energy Management for Multi-Microgrid" 22nd International Middle East Power Systems Conference (MEPCON), pp. 548-555, 2021.

[18] D. Zhou, H. Ding, Q. Wang, and B. Su, "Literature review on renewable energy development and China's roadmap" Frontiers of Engineering Management, DOI: 10.1007/s42524-020-0146-9, Vol. 8, No. 2, pp. 212–222, June 2021.

[19] C. Ammari, D. Belatrache, B. Touhami, and S. Makhloufi, "Sizing, optimization, control and energy management of hybrid renewable energy system—A review" Energy and Built Environment, DOI: 10.1016/j.enbenv.2021.04.002, Vol. 3, No. 4, pp. 339-411, October 2021.

[20] K. El-Naggar, N. H. El-Amary and R. A. Swief, "Optimal Unit commitment using heuristic technique considering environmental effect" 13th International Conference on Electrical Engineering (ICEENG), pp. 47-51, 2022.

[21] R. N. Costandy, S. M. Gasser, M. S. El-Mahallawy, M. W. Fakhr, and S. Y. Marzouk, "P-Wave Detection Using a Fully Convolutional Neural Network in Electrocardiogram Images," Applied Sciences, DOI: 10.3390/app10030976, Vol. 10, No. 3, p. 976, Feberuary 2020.

[22] Z. Cai and C. Peng, "A study on training fine-tuning of convolutional neural networks" 13th International Conference on Knowledge and Smart Technology (KST), Bangsaen, Chonburi, Thailand, pp. 84–89, 2021.

[23] Noureldin S. Eissa and Uswah Khairuddin and Rubiyah Yusof, "A hybrid metaheuristic-deep learning technique for the pan-classification of cancer based on DNA methylation," BMC Bioinformatics, DOI: 10.1186/s12859-022-04815-7, Vol. 23, No. 1, pp. 273, December 2022.

[24] L. Alzubaidi, J. Zhang, A. J. Humaidi, A. Al-Dujaili, Ye Duan, O. Al-Shamma, J. Santamaría, M. A. Fadhel, M. Al-Amidie and L. Farhan, "Review of deep learning: concepts, CNN architectures, challenges, applications, future directions" J Big Data, DOI: 10.1186/s40537-021-00444-8, Vol. 8, No. 1, p. 53, March 2021.

[25] V. X. Son Huu, D. D. Hieu, N. H. Minh Giang, H. Takano and N. D. Tuyen, "Deep Learning-Based Real-Time Solar Irradiation Monitoring and Forecasting Application for PV System," 2023 7th International Conference on Green Energy and Applications (ICGEA), Singapore, Singapore, pp. 40-45, 2023.

[26] A. M. Ibrahim and N. H. El-Amary, "Particle Swarm Optimization trained recurrent neural network for voltage instability prediction," Journal of Electrical Systems and Information Technology, DOI: 10.1016/j.jesit.2017.05.001, Vol. 5, No. 2, pp. 216–228, September 2018.

[27] M. Burgelman, P. Nollet, and S. Degrave, "Modelling polycrystalline semiconductor solar cells" Thin Solid Films, DOI: 10.1016/S0040-6090(99)00825-1, Vol. 361–362, pp. 527–532, Feberuary 2000.

[28] K. Decock, P. Zabierowski, and M. Burgelman,"Modeling metastabilities in chalcopyrite-based thin film solar cells" Journal of Applied Physics, DOI: 10.1063/1.3686651, Vol. 111, No. 4, pp. 1-7, Feberuary 2012.

[29] T. Shawky, M. H. Aly, and M. Fedawy, "Performance Analysis and Simulation of c-Si/SiGe Based Solar Cell" IEEE Access, DOI: 10.1109/ACCESS.2021.3080391, Vol. 9, pp. 75283–75292, 2021.

[30] A. Morales-Acevedo, N. Hernández-Como, and G. Casados-Cruz, "Modeling solar cells: A method for improving their efficiency" Materials Science and Engineering: B, DOI: 10.1016/j.mseb.2012.01.010, Vol. 177, No. 16, pp. 1430–1435, September 2012.